Materials Horizons

ROYAL SOCIETY OF CHEMISTRY

COMMUNICATION

View Article Online
View Journal | View Issue

Check for updates

Cite this: *Mater. Horiz.*, 2025, **12**, 10184

Received 14th May 2025,
Accepted 13th August 2025

DOI: 10.1039/d5mh00912j

rsc.li/materials-horizons

Electro-switchable cellulose nanocrystal films with chiroptical properties

Yota Neagari, †[a] Miguel A. Soto, [a] Yinghao Zhang, [abc] Zongzhe Li, [a] Carl A. Michal [ab] and Mark J. MacLachlan *[acde]

A series of stable electro-switchable cellulose nanocrystal (CNC) films is fabricated by the covalent functionalization of preassembled chiral nematic CNC substrates with electro-active molecules. Through this approach, we anchor siloxy-group-containing viologens (SV) to the surface of CNCs in a preformed film. Unlike conventional premixing strategies that typically disrupt chiral self-assembly of CNCs, this method produces films that retain the structural color and chiroptical properties of the chiral nematic CNC substrate, while exhibiting stable electrochromic performance. Our films show responses not only to voltage but also to light, heat and alkaline environments, demonstrating their potential as multi-responsive materials. This methodology extends beyond chiral nematic CNCs to other nanostructured substrates such as mesoporous chiral nematic silica. The resulting materials show potential for smart optical applications, including dynamic information display and security technologies, enabling tunable visibility and encryption/decryption technologies.

New concepts

We present a post-functionalization strategy for pre-assembled chiral nematic cellulose nanocrystal (CNC) films that enables integration of electro-active molecules without disrupting their hierarchical structure. Conventional pre-mixing methods, especially with cationic species, can interfere with the self-assembly of CNCs and prevent hierarchical ordering into photonic materials. In contrast, our method covalently anchors siloxy viologens onto pre-assembled, chiral nematic CNC films, preserving photonic properties and preventing the leaching of electro-active species. This strategy expands to a range of electro-active molecules and is also applicable to other photonic nanomaterials, such as mesoporous chiral nematic silica. The resulting films exhibit electrochromism while retaining structural color, enabling voltage-dependent modulation of chiroptical signals, which may be useful in chiroptical sensing, anti-counterfeiting materials, and polarized smart windows. Furthermore, the films respond to other stimuli, including light, heat, and base, allowing multi-modal optical switching, which can be useful in the design of sensing devices.

Open Access Article. Published on 15 August 2025. Downloaded on 4/6/2026 6:12:34 AM.
This article is licensed under a Creative Commons Attribution 3.0 Unported Licence.

1. Introduction

Electrochromic (EC) compounds reversibly change their optical properties (*e.g.* absorbance, transmittance, and reflectance) *via* redox reactions under external voltage. These materials have gained substantial interest recently for their use in smart windows, anti-glare mirrors, and displays.[1,2] Combining organic responsive compounds with nanometric scaffolds is a widely used strategy that allows one to harness the properties of the individual components and, in some cases, achieve synergetic behavior or amplified responses. For example, the combination of organic EC compounds with nanomaterials has been shown to improve performance and stability of EC devices, including faster switching speeds, greater cycling stability, and higher contrast.[3–9] While extensive research has been conducted on the combination of EC compounds with low-dimensional nanomaterials (*e.g.* nanoparticles, nanofibers, and nanowires), much less attention has been given to hierarchical nanostructured substrates, such as photonic crystals.[10,11] This approach holds potential for developing materials with uses extending beyond those of standalone EC compounds, yet it remains largely overlooked.

Cellulose nanocrystals (CNCs) are rod-like nanoparticles derived from cellulose, a renewable and biodegradable material obtained from wood pulp, cotton, and other natural resources.[12,13] CNCs are produced through acid hydrolysis, typically using sulfuric acid, which removes the amorphous regions from cellulose microfibrils, leaving behind crystalline domains with high aspect

[a] *Department of Chemistry, University of British Columbia, 2036 Main Mall, Vancouver, BC V6T 1Z1, Canada. E-mail: mmaclach@chem.ubc.ca*
[b] *Department of Physics and Astronomy, University of British Columbia, 6224 Agricultural Rd., Vancouver, BC V6T 1Z1, Canada*
[c] *Stewart Blusson Quantum Matter Institute, University of British Columbia, 2355 East Mall, Vancouver, BC, V6T 1Z4, Canada*
[d] *WPI Nano Life Science Institute, Kanazawa University, Kanazawa, 920-1192, Japan*
[e] *Bioproducts Institute, University of British Columbia, 2360 East Mall, Vancouver, BC, V6T 1Z3, Canada*
† Y. N. is also affiliated with Mitsubishi Materials Corporation, 3-2-3, Marunouchi, Chiyoda-ku, Tokyo, 100-8117, Japan.

This journal is © The Royal Society of Chemistry 2025

Open Access Article. Published on 15 August 2025. Downloaded on 4/6/2026 6:12:34 AM.
This article is licensed under a Creative Commons Attribution 3.0 Unported Licence.

ratios and surface charges introduced by sulfate half-ester groups. Under specific conditions, such as the slow evaporation of aqueous CNC suspensions, these nanoparticles spontaneously self-assemble into chiral nematic structures, forming iridescent films that display structural color and left-handed chiroptical properties.[14–16] These chiral photonic properties have inspired research into advanced materials derived from iridescent CNC films. Furthermore, combining chiral nematic CNC films with stimuli-responsive molecules has demonstrated their potential for creating materials with dynamically tunable optical properties, making them candidates for applications in optical devices, sensors, and information encryption.[17,18]

The combination of chiral nematic CNCs with stimuli-responsive molecules has led to the development of unique adaptive optical materials. While cellulose has advantageous properties such as being biodegradable, lightweight, and inexpensive, which have driven previous research on electrochromic paper,[19–21] examples that integrate electrochromic molecules in chiral nematic CNCs are very limited. For example, one report consists of CNC films co-assembled with an electrochromic polymer (poly(3,4-ethylenedioxythiophene), PEDOT).[22] In this approach, PEDOT and CNCs are part of a composite, but they are not covalently linked to one another. This is limited to PEDOT and restricted to low doping amounts. Large doping concentrations often disrupt the self-assembly of CNCs, preventing the formation of films with chiral nematic order.[23,24] Furthermore, a key challenge in preparing electrochromic chiral nematic CNCs lies in ensuring their stability in electrolyte solutions, as CNC films are prone to swelling and disintegration, leading to leakage of the electroactive components, especially if the dopant is not covalently linked to the substrate.[25,26] Our own group has also succeeded in preparing photochromic composite films by mixing CNCs with electroactive units, but these did not show a chiral nematic structure and were prone to leakage of the electroactive component.[27]

In this study, we develop a new methodology to create stable electro-switchable chiral nematic CNC films through post-modification of chiral nematic CNC substrates by covalently anchoring viologen-containing molecules. Viologens are redox-active species that show excellent reversibility and stability, and their backbone and substituents can be easily tuned, enabling straightforward control over their optical, electrochemical, physical, and chemical properties (Fig. 1(a)).[3,4] Here, we devised a method to functionalize pre-assembled chiral nematic CNC films with siloxy-group-containing viologens (SV), where the siloxy moieties are intended to bond with hydroxyl groups on the surface of the CNC rods.[28–30] Unlike conventional strategies that add electrochromic molecules directly into CNC suspensions, our approach yields films that maintain the structural color and left-handed chiroptical properties of the chiral nematic CNC substrate while exhibiting stable electrochromic performance. Moreover, these films respond not only to voltage but also to light and heat, demonstrating their potential as multi-responsive materials. In addition, we show that this methodology can be extended beyond chiral nematic CNCs to other nanostructured substrates such as mesoporous SiO_2 films.[31–33]

2. Results and discussion

2.1. Fabrication of electrochromic chiral nematic CNC films

Electro-switchable chiral nematic CNC films were fabricated *via* three key steps: film formation, desulfation, and post-functionalization (Fig. 1(b)). In the first step, glucose-containing chiral nematic CNC films (G-CNC) were prepared by slow evaporation of aqueous CNC suspensions (3.9 wt%, pH = 6.6) containing 12.5 wt% glucose relative to CNCs. In these materials, glucose is a sacrificial agent that allows for the infiltration of the precursors needed for functionalization.[34] The second step (desulfation)

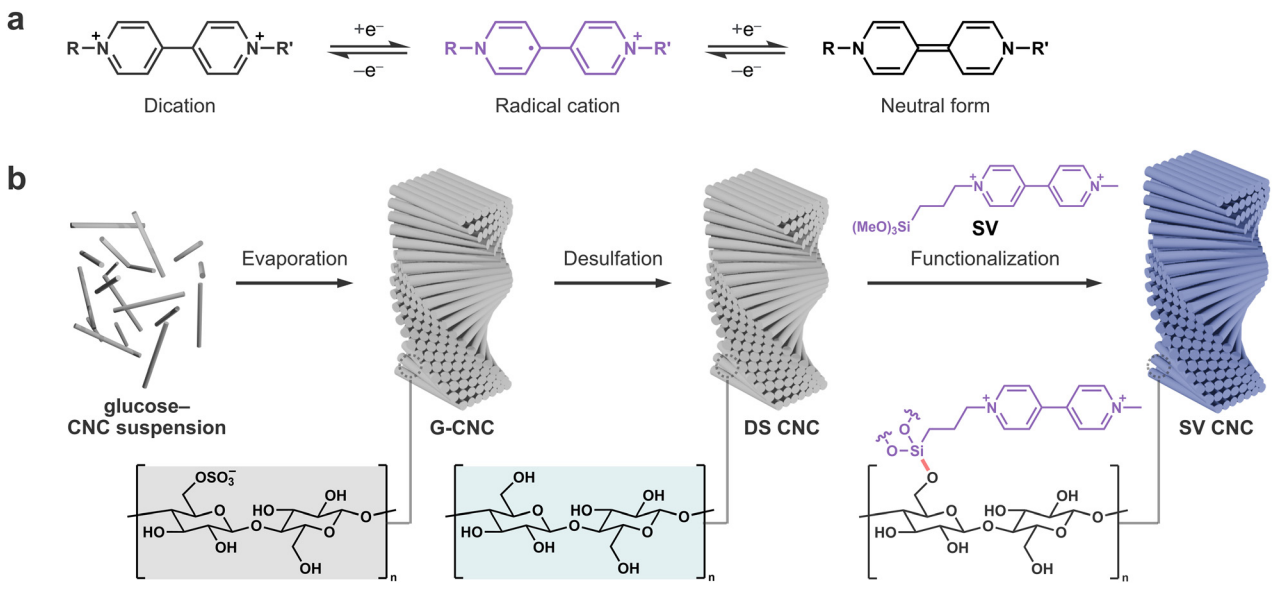

Fig. 1 (a) Reversible redox states of a viologen molecule (counterions omitted for clarity). (b) Schematic illustration of the chiral nematic organization of G-CNC and the preparation of SV CNC *via* desulfation.

Open Access Article. Published on 15 August 2025. Downloaded on 4/6/2026 6:12:34 AM.
This article is licensed under a Creative Commons Attribution 3.0 Unported Licence.

consisted of heating the materials in an alkaline aqueous solution (2 M $NaOH_{(aq)}$, 60 °C) to promote the hydrolysis of the sulfate half-ester groups on the CNC surface and render hydroxyl groups.[35] This step was aimed to reduce the surface charge density on CNCs and enhance hydrogen bonding between adjacent nanorods to improve the stability of the resulting films (desulfated CNC = DS CNC) in aqueous media and humid environments. In the final step, redox-active viologen-containing molecules were covalently attached to the chiral nematic materials. While numerous examples to modify colloidal suspensions of CNCs have been reported, post-functionalization of chiral nematic films has been largely overlooked.[26,36] The desulfated CNC films were immersed in an HCl solution (1 mM, pH = 3.0) containing a siloxy-functionalized viologen (SV, 10 wt% relative to the solution), with DS CNC added at a weight ratio of 1 : 5. The mixture was heated at 50 °C for 4 h. After thorough washing and drying, we obtained the corresponding SV CNC material.

Spectroscopic characterization, *via* FT-IR, UV-vis, and solid-state cross-polarization magic angle spinning (CP-MAS) ^{13}C nuclear magnetic resonance (NMR) spectroscopy, confirmed the successful functionalization of CNC films with SV. The FT-IR spectra of SV CNC films showed a new band at 1508 cm^{-1} and 1563 cm^{-1}, corresponding to the C=C stretching, and a band at 1640 cm^{-1}, corresponding to the C–N stretching from the pyridinium moiety in SV (Fig. S42).[23,27,37] The recorded UV-vis spectrum showed an increase in absorbance intensity below ~300 nm after SV-treatment, corresponding to the characteristic π–π* transition of the dicationic viologen moiety (Fig. S43).[38] Additionally, the ^{13}C CP-MAS NMR spectrum showed signals at 147 and 128 ppm (aromatic carbons), and at 65–9 ppm (alkyl groups), confirming the successful grafting of SV onto CNCs (Fig. S44).[37] Furthermore, elemental analysis revealed a nitrogen content of 0.4 wt% in the SV CNC films, corresponding to a degree of substitution of approximately 0.02 per anhydroglucose unit (AGU), where the degree of substitution represents the average number of substituted hydroxyl groups per AGU and can range from 0 to 3.[39] No nitrogen was detected in either G-CNC or DS CNC films (Table S1). Scanning electron microscopy with energy-dispersive X-ray spectroscopy (SEM-EDX) elemental mapping showed a uniform nitrogen distribution across both the surface and cross-section of the SV CNC film, indicating that the SV functionalization extends throughout the entire film matrix (Fig. S45).

The chiral nematic structure of the CNC films was retained after SV modification. All prepared films are iridescent (Fig. 2(a)); this includes viologen-free (G-CNC and DS CNC), and viologen-containing materials (SV CNC). Polarized optical microscopy (POM) revealed anisotropic textures in each of the films, which is characteristic of chiral nematic order.[14,36] Scanning electron microscopy (SEM) of the cross sections of the films showed characteristic twisted layered structures, typical of chiral nematic assemblies (Fig. S46).[26,36] The average half-pitches of the G-CNC, DS CNC, and SV CNC films (n = 20) measured from the SEM images were 99 ± 11 nm, 110 ± 24 nm, and 111 ± 35 nm, respectively (Table S2). Circular dichroism (CD) measurements revealed intense signals with positive ellipticity, confirming a left-handed chiral nematic structure in the films (Fig. 2(b)).[36] To minimize artifacts from linear dichroism and birefringence, CD spectra were measured using a four-orientation averaging method (Fig. S47).[40] The SV CNC film exhibited a red-shifted CD signal compared to the viologen-free films and had approximately half the intensity. Since SEM analysis showed no significant pitch change, the shift and intensity decrease are attributed to strong UV absorption by the covalently bound SV moieties, which suppress the CD signal in the 300–400 nm region. Notably, composite films

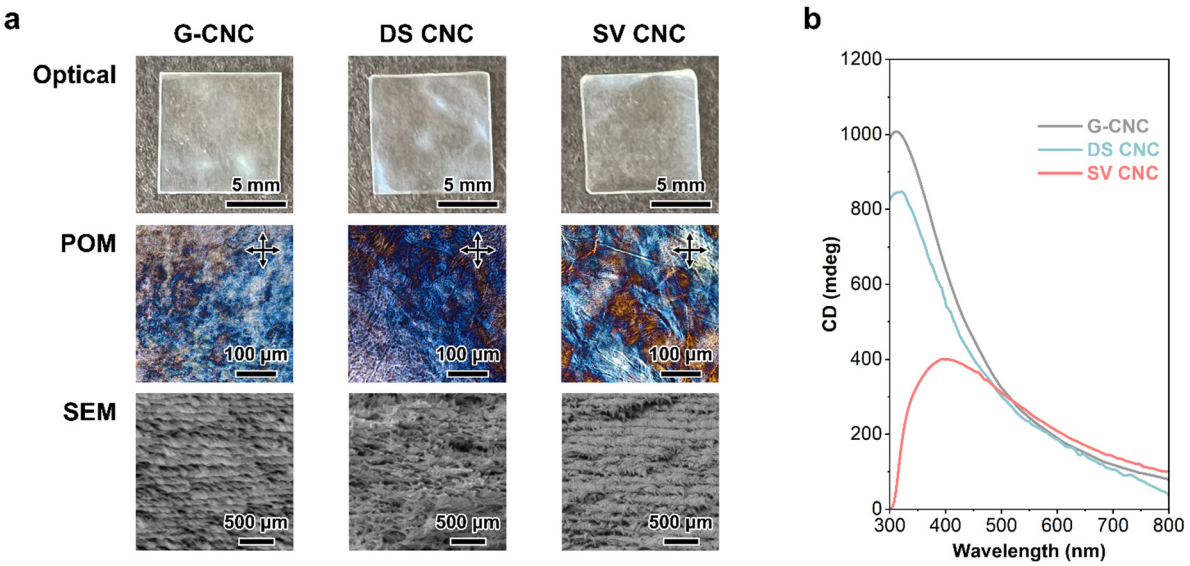

Fig. 2 (a) Optical photographs, polarized optical microscopy (POM) images under crossed polarizers, and scanning electron microscopy (SEM) images for the cross-section of G-CNC, DS CNC, and SV CNC films (10 × 10 mm^2). (b) Circular dichroism (CD) spectra of the CNC films. Each spectrum represents the average of four measurements taken at different orientations (θ = 0°/90°, β = 0°/180°, Fig. S47).

 This journal is © The Royal Society of Chemistry 2025

Open Access Article. Published on 15 August 2025. Downloaded on 4/6/2026 6:12:34 AM.
This article is licensed under a Creative Commons Attribution 3.0 Unported Licence.

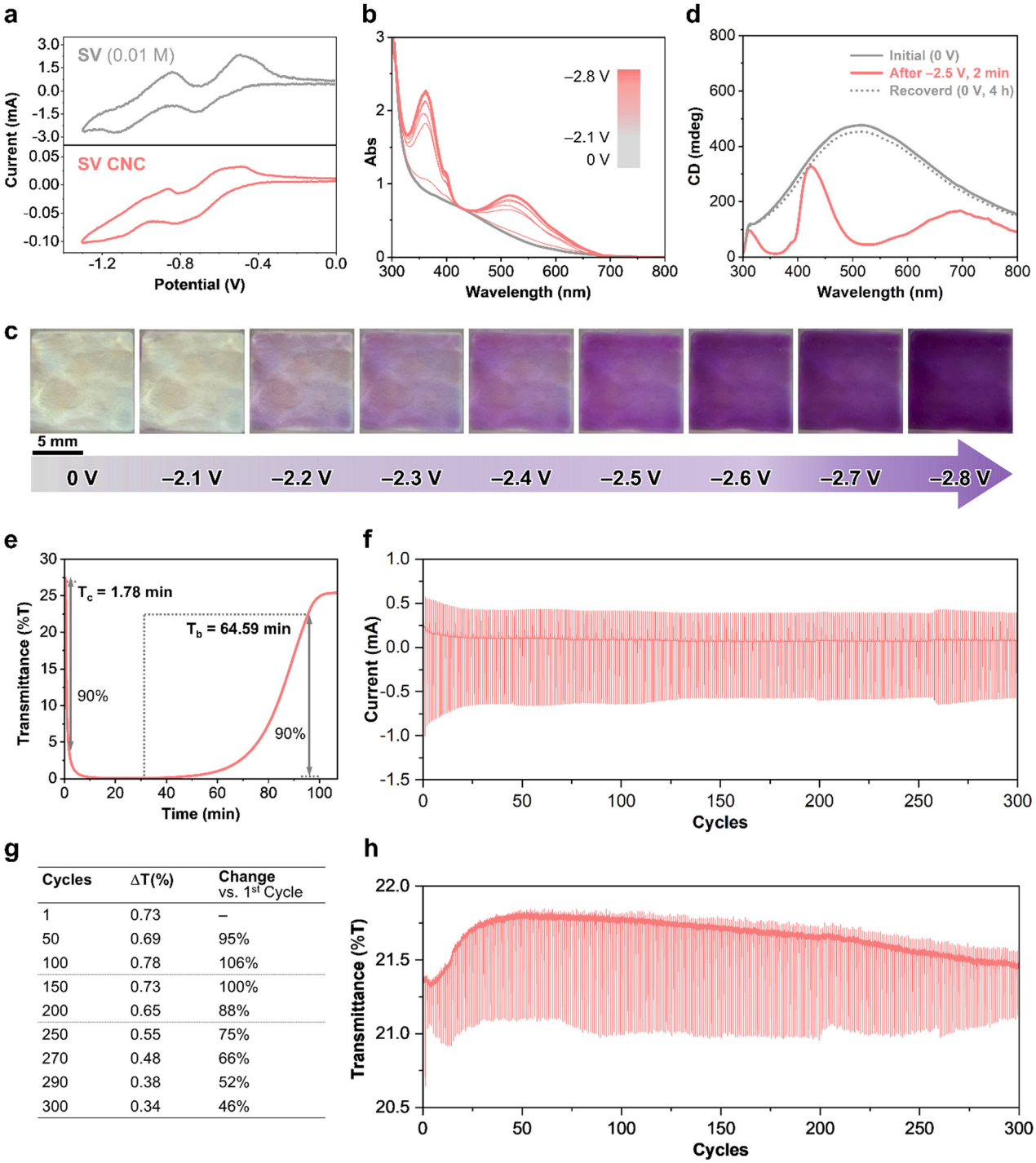

Cycles	ΔT(%)	Change vs. 1st Cycle
1	0.73	–
50	0.69	95%
100	0.78	106%
150	0.73	100%
200	0.65	88%
250	0.55	75%
270	0.48	66%
290	0.38	52%
300	0.34	46%

Fig. 3 (a) Cyclic voltammograms of SV (0.01 M) in KCl (0.1 M) aqueous solution (top) and the SV CNC film in KCl (0.1 M) aqueous solution (bottom), measured using a three-electrode system: ITO glass (working electrode), Pt mesh (counter electrode), Ag/AgCl (reference electrode). (b) UV-vis spectra of the SV CNC film at varying voltages. (c) Optical images of the SV CNC film (10 × 10 mm^2) under different applied voltages. Photographs were taken under ambient light using a standard camera, without the use of polarizers or a microscope. (d) CD spectra of the SV CNC film under 0 V, −2.5 V and after recovery at 0 V. Each spectrum represents the average of four measurements taken at different orientations (θ = 0°/90°, β = 0°/180°, Fig. S56). (e) Transmittance response of the SV CNC film at 520 nm over time under alternating potentials of −2.5 V (31 min) and +2.5 V (76 min). (f)–(h) Cycling stability of the SV CNC film after 300 cycles between −2.5 V for 1 s and +2.8 V for 10 s. (f) Chronoamperometric response. (g) Table showing transmittance change (ΔT) over specific cycles and relative to the first cycle. (h) UV-vis transmittance at 520 nm.

Open Access Article. Published on 15 August 2025. Downloaded on 4/6/2026 6:12:34 AM. This article is licensed under a Creative Commons Attribution 3.0 Unported Licence.

prepared by mixing SV and a CNC suspension did not form a chiral nematic structure (Fig. S48).[23]

Next, we evaluated the stability of the SV CNC films. Static-water contact angle measurements indicated increased hydrophilicity after desulfation and SV treatment, with the contact angle decreasing from 44 ± 1° (G-CNC) to 28 ± 2° (DS CNC) and further to 26 ± 1° (SV CNC) (Fig. S49). Water stability tests showed that G-CNC films swelled and broke down within 3 h, whereas DS CNC and SV CNC films remained stable for over a week (Fig. S50). Thermogravimetric analysis (TGA) revealed that SV CNC films are less thermally stable than G-CNC and DS CNC films with a 10% weight loss registered at 203 °C for G-CNC, 259 °C for DS CNC, and 157 °C for SV CNC, likely due to residual acid from the reaction and washing steps, which may accelerate degradation (Fig. S51).[41] UV-vis spectroscopy confirmed that SV remained in the films after thorough washing or immersion in a 0.1 M potassium chloride solution for one week (Fig. S52). In contrast, methyl viologen (MV), used as a control, leached completely from CNC-MV composite films under the same conditions. This highlights the critical role of covalent functionalization in preventing viologen leakage.

2.2. Electrochromic properties of EC chiral nematic CNC films

The electrochemical behavior of the precursor SV and SV CNC films was investigated using cyclic voltammetry (CV) (Fig. 3(a)). The recorded voltammogram of SV showed the typical reversible two-electron redox process observed for other dicationic viologens.[23,37] The first redox couple at −0.72 V and −0.49 V corresponds to the transformation between the colorless dicationic species (SV^{2+}) and the blue radical cation ($SV^{+\bullet}$).[6,23,42] The second redox couple at −1.12 V and −0.84 V is attributed to electron transfer between the radical cation ($SV^{+\bullet}$) and the fully reduced species (SV^{0}). Similarly, the CV results of SV CNC films exhibited the characteristic redox pairs, confirming the redox activity of the films.

The electrochromic performance of the SV CNC film was evaluated using a device comprising two ITO glasses and a 0.1 M KCl aqueous solution as the electrolyte (Fig. S53). The redox behavior of an SV CNC film in this device was analyzed by CV to determine the voltage range required for coloration and bleaching. A significant increase in peak current was observed starting at approximately −2.1 V on the reducing side and +2.1 V on the oxidizing side (Fig. S54). UV-vis spectra of the SV CNC films in their colored and uncolored states were recorded while the voltage was changed from 0 to −2.8 V. As indicated by the CV results, coloration began at −2.1 V, with bands at 520 nm and 363 nm increasing in absorbance as the voltage increased (Fig. 3(b)). These bands are attributed to viologen radical cations and correspond to a HOMO–SOMO transition and a SOMO–LUMO transition, respectively.[37,42–44] The absorbance and color intensity were found to correlate with the number of reduced SV species, confirming the voltage-dependent electrochromic response of the SV CNC films (Fig. 3(c), and Fig. S55). Similarly, the chiroptical properties of SV CNC films were investigated under applied voltage by CD spectroscopy (Fig. 3(d) and Fig. S56). Upon applying −2.5 V, the CD spectrum changed from a single broad band to a spectrum with lower intensities at 520 nm and 363 nm, corresponding to the absorption of the reduced viologen (observed in the UV-vis spectrum). After removing the applied voltage (0 V), the recorded CD spectrum was reminiscent of that initially observed, demonstrating reversible chiroptical behavior. The reversible change in the CD response was observed over multiple cycles (4 cycles), confirming its repeatability and cycling stability (Fig. S57). It is worth noting that although SV is achiral and exhibits no CD signal on its own (Fig. S58), its interaction with the chiral nematic CNC induces a chiroptical response that reversibly changes with voltage. This behavior arises from the viologen molecules, significantly smaller than CNCs, being incorporated into the chiral structure and aligning along the chiral nematic framework, leading to chiral induction with enhanced optical activity.[45] This interaction enables voltage-controlled modulation of the CD signal, emphasizing the tunability of chiroptical properties through electrochemical switching.

The switching speed of EC materials is generally defined as the time required for a 90% change in transmittance.[1] The switching speed of a SV CNC film was evaluated (Fig. 3(e)), finding that it reaches 90% coloration (T_c) in 1.8 minutes at −2.5 V, with 90% recovery (T_b) back to its uncolored state in 64.6 minutes at +2.5 V. Importantly, the film showed good memory retention, maintaining its color for over 64 minutes under +2.5 V. With this performance, the films may be suitable for applications in, *e.g.* smart windows, where memory retention is more important than rapid switching.[10] In addition, the film retained 75% of its initial performance after 250 cycles (Fig. 3(f)–(h)) and showed only a significant decay in cycle 259, with performance declining to 46% by cycle 300. Films prepared by treating G-CNC with SV without desulfation exhibited swelling in the electrolyte and degraded more rapidly during cycling tests compared to SV CNC films (Fig. S59).

After demonstrating that our method allows for the incorporation of electroactive species in chiral nematic CNC films, we explored the color tunability of the materials by incorporating viologens containing different substituents.[3,4,9] Siloxy viologens with *p*-trifluoromethylphenyl (CF_3SV) and *p*-cyanophenyl (CNSV) groups were synthesized and CF_3SV CNC and CNSV CNC films were prepared using the same method described for SV CNC films (Fig. 4(a) and (b)). The reduction of CF_3SV CNC and CNSV CNC produced purple and blue films, respectively. Coloration began around −2.1 V (determined by CV, Fig. S60), with absorption bands appearing at 560 nm and 390 nm for CF_3SV CNC, and at 580 nm and 425 nm for CNSV CNC, both showing increased absorbance with increasing applied voltage, similar to SV CNC (Fig. S61 and S62). The sequential red shift from SV CNC to CF_3SV CNC and CNSV CNC can be attributed to the stronger electron-withdrawing effects of the *p*-trifluoromethylphenyl and *p*-cyanophenyl groups compared to the methyl group, which lower the LUMO level, reducing the band gap and shifting absorption to longer wavelengths.[9] These findings demonstrate that the electrochromic color of CNC films can be tuned by altering the viologen structure. With readily available electrochemical control to switch the color ON and OFF in our

 This journal is © The Royal Society of Chemistry 2025

Open Access Article. Published on 15 August 2025. Downloaded on 4/6/2026 6:12:34 AM.
This article is licensed under a Creative Commons Attribution 3.0 Unported Licence.

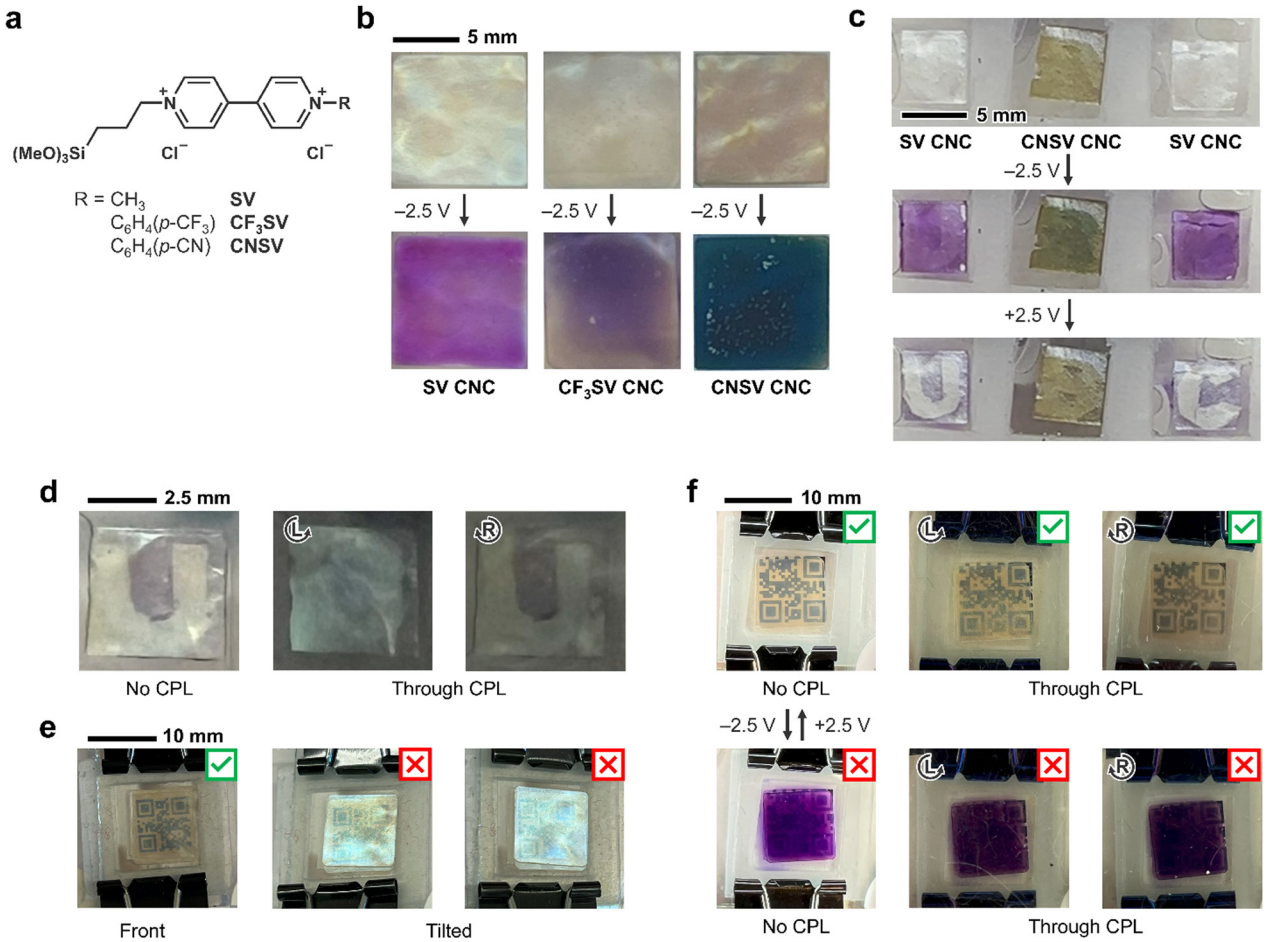

Fig. 4 (a) Chemical structures of SV, CF_3SV, and CNSV. (b) Photographs of CNC films (10 × 10 mm^2) treated with different viologens, showing their electrochromic color responses: SV CNC, CF_3SV CNC, and CNSV CNC films, respectively. (c) and (d) Demonstration of hidden text revealed through electrochemistry. (c) Photographs of a multicolor hidden text device constructed with SV CNC and CNSV CNC films (5 × 5 mm^2) under different applied voltages, taken under ambient light without optical filters. (d) Photographs of the hidden text device viewed without circularly polarized (CPL) filters and with right-handed and left-handed CPL filters. (e) and (f) A dynamic QR code display constructed using double-layered SV CNC films (10 × 10 mm^2). (e) Photographs of a dynamic QR code displays with different viewing angles without optical filters. (f) Photographs of a dynamic QR code display under different applied voltages, viewed without CPL filters and with right-handed and left-handed CPL filters.

materials, we envisioned that these films could be useful in information encryption and security displays. A device was constructed by sandwiching SV CNC and CNSV CNC films between ITO glass electrodes, with a polyethylene terephthalate film cut into "U," "B," and "C" placed beneath the CNC films (Fig. S63, S64 and Video S1). When −2.5 V was applied with the front side as the cathode, the CNC films became uniformly colored (Fig. 4(c)). Reversing the voltage selectively colored only the regions in contact with the ITO glass, revealing the masked letters. Reapplying −2.5 V restored uniform coloration, concealing the text. Readability was further controlled using circular polarization (CPL) filters: an R-CPL filter enhanced contrast, while an L-CPL filter reduced visibility by emphasizing the iridescent reflection of the CNC films (Fig. 4(d)).[24]

Additionally, a dynamic QR code display was constructed by assembling a device with a double-layered SV CNC film and positioning a QR code on the backside (Fig. S65 and Video S2). Due to the angle-dependent iridescent reflection of the CNC films, the QR code was readable from certain angles but became unreadable when the viewing angle changed as the reflection intensified (Fig. 4(e)). When a voltage was applied, coloring the SV CNC films, the QR code became unreadable. However, applying the reverse voltage restored the films to their original state, making the QR code readable again (Fig. 4(f)). A CPL filter had no effect on readability in either state. These devices show potential of electrochromic CNC films for dynamic information display and security applications, enabling tunable visibility and encryption capabilities.

2.3. Other stimuli

Viologen compounds are widely known for their responsiveness to multiple stimuli, including electricity, light, heat, and bases.[3,4,27,46–49] With this in mind, we sought to explore the multi-responsiveness of SV-modified CNC materials. Films prepared by treating G-CNC with SV without desulfation demonstrated reversible photochromic and thermochromic properties, with distinct color depending on the applied stimulus (Fig. 5(a), (b) and Fig. S66, S67). Upon exposure to 302 nm UV light, the

Open Access Article. Published on 15 August 2025. Downloaded on 4/6/2026 6:12:34 AM.
This article is licensed under a Creative Commons Attribution 3.0 Unported Licence.

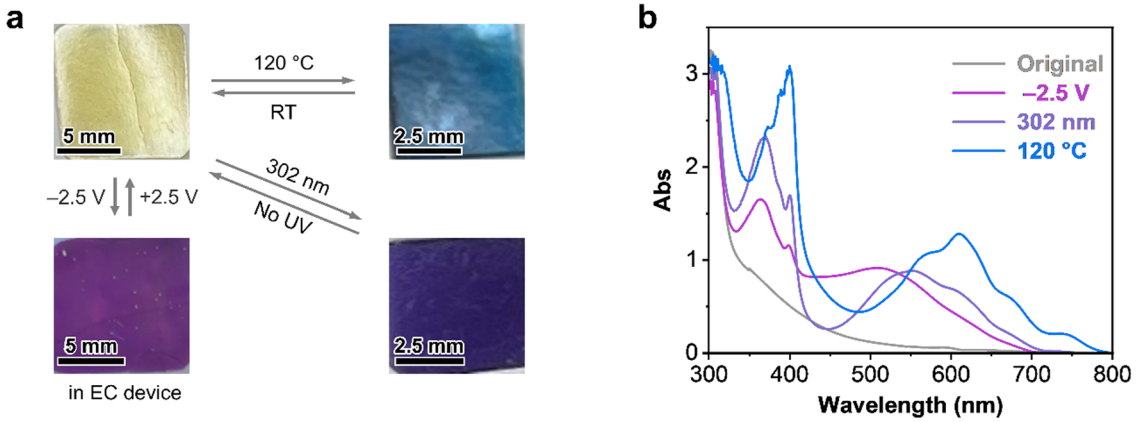

Fig. 5 (a) Photographs of SV CNC films (10 × 10 mm^2 and 5 × 5 mm^2) responding to heat, light, and electricity. (b) UV-vis spectra of SV CNC films under different stimuli.

films turned to a vibrant purple-blue, with UV-vis bands appearing at 550 nm and 370 nm. Heating at 120 °C resulted in a blue color, with absorption peaks shifted to 610 nm and 400 nm. These spectral changes suggest that the ratio of reduced viologen species varies depending on the stimulus. Upon reduction, viologen radical cations generally exist in equilibrium between monomeric and π–π-interacting dimeric forms. The dimers absorb at longer wavelengths than the monomers, causing an apparent red shift as their proportion increases. This behavior has been reported both in solution and for viologens immobilized on solid substrates.[37,42–44] Therefore, the observed stimulus-dependent spectral shifts likely reflect changes in the monomer–dimer equilibrium under different stimuli.[49,50] The colored films gradually returned to their original color after 1–7 days once the stimuli were removed. SV CNC films prepared through desulfation exhibited photochromic properties and color changes under UV irradiation but turned brown upon heating and did not exhibit reversible thermochromic behavior (Fig. S68 and S69). This irreversible color change may be caused by residual acid from the HCl washing step, which could promote acid-catalyzed thermal degradation of cellulose.[51] Supporting this hypothesis, DS CNC films without SV treatment also exhibited thermal discoloration when heated (Fig. S68c). Similar to our observations in the electro-responsive materials, UV irradiation and heating led to stimulus-specific decreases in CD signal intensity, occurring around 520/370 nm and 610/400 nm, respectively, corresponding to the UV-vis absorption bands of the reduced form of the viologen (Fig. S70 and S71). Additionally, the SV CNC films turned purple in 2 M $NaOH_{(aq)}$, where the base acted as an electron donor, reducing viologen dications to radical cations with strong visible absorption (Fig. S72).[48] The ability of these films to respond to multiple stimuli highlights their versatility and potential for use in fields requiring multi-functional materials.

2.4. Extending electrochromic functionality to chiral nematic mesoporous materials

The chiral nematic organization of CNCs can be transferred to other materials, such as silica, titania, and carbon, through templating, allowing one to create various chiral nematic mesoporous materials with interesting nanostructures and chiroptical properties.[31–33] For example, chiral nematic mesoporous silica (CNMS) can be synthesized by introducing a silica precursor into a CNC suspension, followed by an evaporation process and subsequent removal of CNCs *via* calcination or acid hydrolysis to yield iridescent films. Previous studies have demonstrated that CNMS films can be further functionalized through post-modification, with examples including the introduction of thermo-responsive, photoresponsive, and hydrophobic properties.[52–54] The feasibility of extending the approach to impart electrochromic properties through post-functionalization of chiral nematic CNCs to other chiral nematic mesoporous materials was investigated. To the best of our knowledge, this is the first example introducing electroactive components into chiral nematic silica, highlighting its potential as a platform for novel materials that combine unique responsive, optical and porous properties.

SV CNMS films were fabricated by modifying CNMS films prepared using an existing method with SV (Fig. 6(a)).[31,32] Chiral nematic CNC/SiO_2 composite films were prepared by the evaporation of a CNC suspension (4.0 wt%, pH = 2.0) containing tetramethyl orthosilicate (TMOS) as a silica precursor (CNC : TMOS = 1.0 : 1.3 w/w). The CNC template was then removed by acid hydrolysis with sulfuric acid, followed by piranha solution (30% H_2O_2 : H_2SO_4 = 1 : 5 v/v), yielding CNMS films. The obtained CNMS films were immersed in an HCl solution (pH = 3.0) containing SV (5 wt%, CNMS : SV = 1 : 5 w/w) and heated at 50 °C. After thorough washing and drying, the corresponding SV CNMS films were obtained.

The SV modification of the resulting films was confirmed by FT-IR, UV-vis, and ^{13}C CP-MAS NMR. Similar to SV CNC films, FT-IR spectra showed new peaks at 1508 cm^{-1} and 1563 cm^{-1} (C═C stretching) and 1640 cm^{-1} (C═N stretching) (Fig. S73). UV-vis spectra exhibited increased absorption below ∼300 nm (Fig. S74), and ^{13}C CP-MAS NMR revealed signals corresponding to SV moieties (Fig. S75). The chiral nematic structure of CNMS films was preserved after SV modification, as confirmed by the visible iridescent color, anisotropic textures observed in POM, characteristic twisted layered structures in SEM, and strong positive signals in CD, confirming a left-handed chiral

 This journal is © The Royal Society of Chemistry 2025

Open Access Article. Published on 15 August 2025. Downloaded on 4/6/2026 6:12:34 AM.
This article is licensed under a Creative Commons Attribution 3.0 Unported Licence.

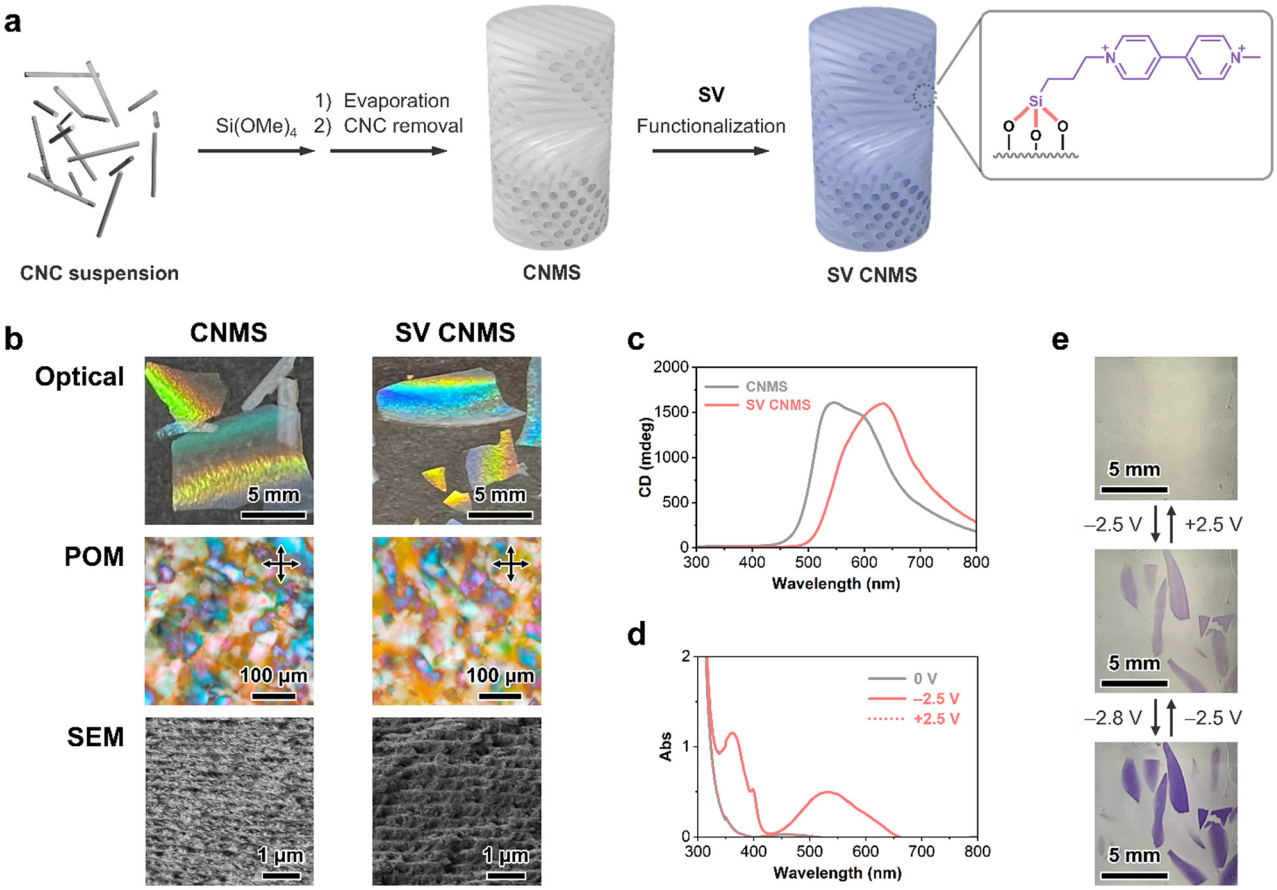

Fig. 6 (a) Schematic illustration of the fabrication of CNMS and SV CNMS films. (b) Optical photographs, POM images under crossed polarizers, and SEM cross-sectional images of CNMS and SV CNMS films. (c) CD spectra of CNMS and SV CNMS films. Each spectrum represents the average of four measurements taken at different orientations (θ = 0°/90°, β = 0°/180°, Fig. S77). (d) UV-vis spectra of SV CNMS films at 0 V, −2.5 V and after recovery at +2.5 V. (e) Optical images of SV CNMS films under different applied voltages, taken under ambient light without optical filters.

nematic structure in all films (Fig. 6(b), (c) and Fig. S76, S77, Table S3).[31,32,52–54] For the electrochromic performance of SV CNMS, CV measurements revealed a significant increase in peak current starting at approximately −2.1 V on the reducing side and +2.1 V on the oxidizing side (Fig. S78). Upon applying voltage to the SV CNMS films in 0.1 M KCl aqueous electrolyte, UV-vis analysis showed that the absorption bands at 520 nm and 363 nm increased proportionally to the applied voltage, resulting in a purple coloration (Fig. 6(d) and (e)). When the CNMS films absorb water, the refractive indices of the liquid within the pores and silica walls become nearly identical, rendering the film colorless and transparent.[31] This refractive index match also diminishes the CD signal significantly, so no distinct voltage-dependent chiroptical changes were observed in the SV CNMS films (Fig. S79 and S80). To further evaluate the electrochromic performance of SV CNMS films, switching speed and cycling stability were assessed (Fig. S81). The film achieved 90% coloration (T_c) in 5.9 minutes at −2.5 V and 90% bleaching (T_b) in 21 minutes at +2.5 V. The cycling stability of the SV CNMS film was lower than that of the SV CNC film, with the performance dropping to 28% of its initial performance after only 50 cycles (*vs.* 95% for the SV CNC film). TGA analysis showed that SV CNMS films are thermally stable, with 10% weight loss registered at 300 °C (Fig. S82). This method demonstrates the feasibility of incorporating electrochromic functionality into various substrates, including a chiral nematic glass.

3. Conclusions

This study presents a new method for the fabrication of electro-switchable chiral nematic CNC films by covalently anchoring siloxy-group-containing viologens as electro-active molecules onto pre-assembled CNC substrates. Unlike conventional approaches, this post-functionalization method preserves the chiral nematic structure while imparting stable and reversible electroactivity. The resulting films exhibit a unique combination of electrochromic and chiroptical properties, as demonstrated by their voltage-dependent CD spectra. With electrochemical control over color switching, these materials were used to construct functional devices, such as hidden text displays and dynamic QR codes, highlighting their potential for information encryption and security applications. Additionally, tuning the viologen structure enables precise adjustment of the colorful readouts. Beyond electrochromism, the films also respond to heat, light, and base. Although not all of them showed reversible

Open Access Article. Published on 15 August 2025. Downloaded on 4/6/2026 6:12:34 AM. This article is licensed under a Creative Commons Attribution 3.0 Unported Licence.

thermochromism, the materials demonstrate multi-responsive behavior. Our methodology extends beyond CNC-based films to other nanostructured substrates, such as SiO_2, broadening its applicability. By integrating electrochromic molecules with hierarchical nanostructures, this work presents an alternative for the fabrication of smart optical materials with tunable, responsive, and nanostructure-based properties, including structural color and chiroptical properties.

Author contributions

Y. N. designed the experiments, prepared samples, conducted the majority of measurements and analysis, and wrote the original draft of the manuscript. M. A. S. contributed to the conceptualization of the project, supported methodology development, and co-wrote the manuscript. Y. Z. assisted with sample preparation and characterization. Y. Z. and C. A. M. performed solid-state NMR experiments and data analysis. Z. L. contributed to SEM analysis and performed SEM-EDX analysis. M. J. M. supervised the project, provided valuable feedback, acquired funding, contributed resources, and reviewed and revised the manuscript.

Conflicts of interest

There are no conflicts to declare.

Data availability

All experimental procedures, characterisation data, supporting spectra, electron micrographs, and other data can be found in the article or in the SI. Supporting videos for this work are available to demonstrate the applications: supporting video 1 (multicolor hidden text device) and supporting video 2 (dynamic QR code display). See DOI: **https://doi.org/10.1039/d5mh00912j**

Acknowledgements

This work was supported by the Natural Sciences and Engineering Research Council (NSERC) of Canada (Discovery Grant) and Mitsubishi Materials Corporation. MJM thanks the Canada Research Chair Program for support and acknowledges the Canada Foundation for Innovation (CFI) and British Columbia Knowledge Development Fund (BCKDF) for infrastructure grants (JELF 34098, 38963). We thank Wadood Hamad (formerly at FPInnovations) for providing the CNCs used to make the CNMS. The authors gratefully acknowledge UBC Bioimaging Facility (Derrick Horne, RRID: SCR_021304) for training and assistance with SEM, and the UBC Chemistry Shared Instrument Facility (Benjamin Herring) for training and assistance with FTIR, TGA, and CD, and the Mass Spectrometry and Microanalytical Laboratory at UBC for conducting high-resolution mass spectrometry and elemental analysis measurements. We also thank Lucas J. Andrew (UBC) for assistance with POM analysis, and Seiya Ota (UBC) for mass spectrometry analysis.

References

1 C. Gu, A.-B. Jia, Y.-M. Zhang and S. X.-A. Zhang, *Chem. Rev.*, 2022, **122**, 14679–14721.
2 S. Wu, H. Sun, M. Duan, H. Mao, Y. Wu, H. Zhao and B. Lin, *Cell Rep. Phys. Sci.*, 2023, **4**, 101370.
3 M. Grätzel, *Nature*, 2001, **409**, 575–576.
4 L. Striepe and T. Baumgartner, *Chem. – Eur. J.*, 2017, **23**, 16924–16940.
5 N. Vlachopoulos, J. Nissfolk, M. Möller, A. Briançon, D. Corr, C. Grave, N. Leyland, R. Mesmer, F. Pichot, M. Ryan, G. Boschloo and A. Hagfeldt, *Electrochim. Acta*, 2008, **53**, 4065–4071.
6 E. Hwang, S. Seo, S. Bak, H. Lee, M. Min and H. Lee, *Adv. Mater.*, 2014, **26**, 5129–5136.
7 T. Kuno, Y. Matsumura, K. Nakabayashi and M. Atobe, *Angew. Chem., Int. Ed.*, 2016, **55**, 2503–2506.
8 S. Mishra, S. Lambora, P. Yogi, P. R. Sagdeo and R. Kumar, *ACS Appl. Nano Mater.*, 2018, **1**, 3715–3723.
9 Y. Choi, K.-W. Kim, Y. R. In, X. Tang, P. Kim, V. H. V. Quy, Y. M. Kim, J. Lee, C. Choi, C. Jung, S. H. Kim, H. C. Moon and J. K. Kim, *Chem. Eng. J.*, 2022, **429**, 132319.
10 G. Yang, Y.-M. Zhang, Y. Cai, B. Yang, C. Gu and S. X.-A. Zhang, *Chem. Soc. Rev.*, 2020, **49**, 8687–8720.
11 L. Li, Z. Yu, C. Ye and Y. Song, *Adv. Funct. Mater.*, 2024, **34**, 2311845.
12 Y. Habibi, L. A. Lucia and O. J. Rojas, *Chem. Rev.*, 2010, **110**, 3479–3500.
13 Z. Chen, Y. Hu, G. Shi, H. Zhuo, M. A. Ali, E. Jamróz, H. Zhang, L. Zhong and X. Peng, *Adv. Funct. Mater.*, 2023, **33**, 2214245.
14 J.-F. Revol, H. Bradford, J. Giasson, R. H. Marchessault and D. G. Gray, *Int. J. Bio. Macromol.*, 1992, **14**, 170–172.
15 A. Tran, C. E. Boott and M. J. MacLachlan, *Adv. Mater.*, 2020, **32**, 1905876.
16 B. Frka-Petesic, T. G. Parton, C. Honorato-Rios, A. Narkevicius, K. Ballu, Q. Shen, Z. Lu, Y. Ogawa, J. S. Haataja, B. E. Droguet, R. M. Parker and S. Vignolini, *Chem. Rev.*, 2023, **123**, 12595–12756.
17 D. Qu, O. J. Rojas, B. Wei and E. Zussman, *Adv. Opt. Mater.*, 2022, **10**, 2201201.
18 S. Singh, S. Bhardwaj, N. Choudhary, R. Patgiri, Y. Teramoto and P. K. Maji, *ACS Appl. Mater. Interfaces*, 2024, **16**, 41743–41765.
19 A. Malti, R. Brooke, X. Liu, D. Zhao, P. Andersson Ersman, M. Fahlman, M. P. Jonsson, M. Berggren and X. Crispin, *J. Mater. Chem. C*, 2016, **4**, 9680–9686.
20 A. Viñuales, Y. Alesanco, G. Cabañero, J. Sobrado and R. Tena-Zaera, *Sol. Energy Mater.*, 2017, **167**, 22–27.
21 A. W. Lang, A. M. Österholm and J. R. Reynolds, *Adv. Funct. Mater.*, 2019, **29**, 1903487.
22 K. Feng, M. Lu, G. Wei, F. Tang and Z. Jin, *ACS Appl. Nano Mater.*, 2022, **5**, 10848–10859.

 This journal is © The Royal Society of Chemistry 2025

Open Access Article. Published on 15 August 2025. Downloaded on 4/6/2026 6:12:34 AM. This article is licensed under a Creative Commons Attribution 3.0 Unported Licence.

23 Y. Su, F. Yang, L. Zhou, Y. Geng, J. Zhang and M. Jiang, *ChemElectroChem*, 2018, **5**, 1407–1414.
24 J. Fan, M. Xu, Y.-T. Xu, W. Y. Hamad, Z. Meng and M. J. MacLachlan, *Chem. Eng. J.*, 2023, **457**, 141175.
25 F. Zhang, W. Ge, C. Wang, X. Zheng, D. Wang, X. Zhang, X. Wang, X. Xue and G. Qing, *ACS Appl. Mater. Interfaces*, 2021, **13**, 17118–17128.
26 Z. Li, P. Wang, Y. Zhang, C. A. Michal and M. J. MacLachlan, *Small*, 2025, **21**, 2409701.
27 Y. Shi, M. A. Soto, Z. Li and M. J. MacLachlan, *New J. Chem.*, 2024, **48**, 10588–10592.
28 A. Dufresne, *Mater. Today*, 2013, **16**, 220–227.
29 M. Abdelmouleh, S. Boufi, A. Ben Salah, M. N. Belgacem and A. Gandini, *Langmuir*, 2002, **18**, 3203–3208.
30 F. Ludovici, R. Hartmann and H. Liimatainen, *Cellulose*, 2023, **30**, 775–787.
31 K. E. Shopsowitz, H. Qi, W. Y. Hamad and M. J. MacLachlan, *Nature*, 2010, **468**, 422–425.
32 K. E. Shopsowitz, W. Y. Hamad and M. J. MacLachlan, *J. Am. Chem. Soc.*, 2012, **134**, 867–870.
33 J. A. Kelly, M. Giese, K. E. Shopsowitz, W. Y. Hamad and M. J. MacLachlan, *Acc. Chem. Res.*, 2014, **47**, 1088–1096.
34 C. E. Boott, M. A. Soto, W. Y. Hamad and M. J. MacLachlan, *Adv. Funct. Mater.*, 2021, **31**, 2103268.
35 N. Lin and A. Dufresne, *Nanoscale*, 2014, **6**, 5384–5393.
36 E. Lizundia, T.-D. Nguyen, J. L. Vilas, W. Y. Hamad and M. J. MacLachlan, *J. Mater. Chem. A*, 2017, **5**, 19184–19194.
37 A. Ruff, P. Schuler and B. Speiser, *J. Solid State Electrochem.*, 2013, **17**, 79–97.
38 B. C. De Simone, T. Marino and N. Russo, *Theor. Chem. Acc.*, 2016, **135**, 118.
39 T. Heinze and T. Liebert, *Prog. Polym. Sci.*, 2001, **26**, 1689–1762.
40 Y. Yao, T. J. Ugras, T. Meyer, M. Dykes, D. Wang, A. Arbe, S. Bals, B. Kahr and R. D. Robinson, *ACS Nano*, 2022, **16**, 20457–20469.
41 F. D'Acierno, W. Y. Hamad, C. A. Michal and M. J. MacLachlan, *Biomacromolecules*, 2020, **21**, 3374–3386.
42 E. M. Kosower and J. L. Cotter, *J. Am. Chem. Soc.*, 1964, **86**, 5524–5527.
43 E. Borgarello, E. Pelizzetti, W. A. Mulac and D. Meisel, *J. Chem. Soc., Faraday Trans. 1*, 1985, **81**, 143.
44 K. Nchimi-Nono, P. Dalvand, K. Wadhwa, S. Nuryyeva, S. Alneyadi, T. Prakasam, A. C. Fahrenbach, J. Olsen, Z. Asfari, C. Platas-Iglesias, M. Elhabiri and A. Trabolsi, *Chem. – Eur. J.*, 2014, **20**, 7334–7344.
45 S. Kang, Y. Li, D. Bukharina, M. Kim, H. Lee, M. L. Buxton, M. J. Han, D. Nepal, T. J. Bunning and V. V. Tsukruk, *Adv. Mater.*, 2021, **33**, 2103329.
46 K. W. Shah, S.-X. Wang, D. X. Y. Soo and J. Xu, *Polymers*, 2019, **11**, 1839.
47 J. Ding, C. Zheng, L. Wang, C. Lu, B. Zhang, Y. Chen, M. Li, G. Zhai and X. Zhuang, *J. Mater. Chem. A*, 2019, **7**, 23337–23360.
48 W. Shi, F. Xing, Y.-L. Bai, M. Hu, Y. Zhao, M.-X. Li and S. Zhu, *ACS Appl. Mater. Interfaces*, 2015, **7**, 14493–14500.
49 D.-X. Xia, C.-Y. Xu, M.-F. Ye, R.-L. Lin and J.-X. Liu, *ACS Appl. Mater. Interfaces*, 2024, **16**, 45745–45753.
50 X.-N. Li, Z.-M. Tu, L. Li, Z.-H. Wang and H. Zhang, *Dalton Trans.*, 2020, **49**, 3228–3233.
51 O. M. Vanderfleet, M. S. Reid, J. Bras, L. Heux, J. Godoy-Vargas, M. K. R. Panga and E. D. Cranston, *Cellulose*, 2019, **26**, 507–528.
52 M. Giese, J. C. De Witt, K. E. Shopsowitz, A. P. Manning, R. Y. Dong, C. A. Michal, W. Y. Hamad and M. J. MacLachlan, *ACS Appl. Mater. Interfaces*, 2013, **5**, 6854–6859.
53 A. S. Terpstra, W. Y. Hamad and M. J. MacLachlan, *Adv. Funct. Mater.*, 2017, **27**, 1703346.
54 J. K. Szymkowiak, C. M. Walters, W. Y. Hamad and M. J. MacLachlan, *Eur. J. Inorg. Chem.*, 2022, e202200218.